Sizing and Analysis of Renewable Energy and Battery Systems in Residential Microgrids

Raji Atia and Noboru Yamada, *Member, IEEE*

***Abstract*—Accelerated development of eco-friendly technologies such as renewable energy, smart grids, and electric transportation will shape the future of electric power generation and supply. Accordingly, the power consumption characteristics of modern power systems are designed to be more flexible, which impact the system sizing. However, integrating these considerations into the design stage can be complex. Under these terms, this paper presents a novel model based on mixed integer linear programming for the optimization of a hybrid renewable energy system with a battery energy storage system in residential microgrids in which the demand response of available controllable appliances is coherently considered in the proposed optimization problem with reduced calculation burdens. The model takes into account the intrinsic stochastic behavior of renewable energy and the uncertainty involving electric load prediction, and thus proper stochastic models are considered. This paper investigates the effect of load flexibility on the component sizing of the system for a residential microgrid in Okinawa. Also under consideration are different operation scenarios emulating technical limitations and several uncertainty levels.**

***Index Terms*—Design optimization, demand response, hybrid power systems, microgrids, performance analysis.**

I. Nomenclature

$B_{Aq}, B_{O\&M}, B_{Rep}$	Annualized acquisition, operating, and replacement costs of the battery ($/kWh).
$C_P(t), C_S(t)$	Prices of purchasing and selling electricity at t ($/kWh).
D_{App}^{m}	Task commitment duration of an appliance type m (h).
$Inv_{Aq}, Inv_{O\&M}$, *and* Inv_{Rep}	Annualized acquisition, operating, and replacement costs of the inverter ($/kW).
i, m	Indices of appliance types.
$K_{i,m}, F_{i,m}$	Factors related to the commitment of appliance type m during $\mathcal{H}_i$.
N_{App}^{m}	Number of appliances of type m.
N_B	Installed battery capacity (kWh).
N_{Inv}	Installed capacity of the bi-directional inverter (kW).
N_{PV}	Installed capacity of the PV array (kW)
N_{WT}	Installed capacity of wind turbines (kW).
$PV_{Aq}, PV_{O\&M}$	Annualized acquisition and operating costs of PV ($/kW).
P_{App}^{m}	Average power consumed by an online appliance m (kW).
$\overline{P_B}$	Battery maximum charge/discharge power per kWh (kW).
$P_{Ch}(t), P_{Dch}(t)$	Battery charged and discharged power at t (kW).
$\overline{P_G}$	Maximum grid power that can be purchased or sold (kW).
P_{PG}	Hourly grid purchased power (kW).
$P_L(t)$	Total power consumption at t (kW).
$P_{NCL}(t)$	Non-controllable load power at t (kW).
$P_{PG}^{ac}(t)$	Grid-purchased power, dispatched to supply the load at t (kW).
$P_{PG}^{dc}(t)$	Grid purchased power, dispatched to the DC side for charging the battery at t (kW).
P_{PV}	Hourly generated power by installed PVs (kW).
$P_{PV}^{ac}(t)$	PV power dispatched to AC at t (kW).
$P_{PV}^{dc}(t)$	PV power dispatched to charge the battery at t (kW).
$P_{PV_1}(t)$	Generated power by equivalent 1 kW PV at t (kW).
$P_{SG}(t)$	Power sold to the grid at t (kW).
P_{WT}	Hourly generated power by installed WTs (kW).
$P_{WT}^{ac}(t)$	WT power dispatched directly to the AC side at t (kW).
$P_{WT}^{dc}(t)$	WT power dispatched to DC to charge the battery at t (kW).
$P_{WT_1}(t)$	Generated power by equivalent 1 kW WT at t (kW).
$Q_B(t)$	Battery stored energy at the beginning of the t th hour (kWh).
$Q_f(t)$	Battery capacity fade at the beginning of the t th hour (kWh).
$\underline{SOC}$	Minimum allowed state of charge for the battery.
$\overline{SOC}$	Maximum allowed state of charge.
SOC_0	Initial state of charge of the battery at the beginning of the optimization period.

Manuscript received September 27, 2014; revised October 19, 2015 and December 5, 2015; accepted January 14, 2016. Date of publication February 3, 2016; date of current version April 19, 2016. Paper no. TSG-00959-2014.

The authors are with the Graduate School of Energy and Environment Science, Nagaoka University of Technology, Nagaoka 940-2188, Japan (e-mail: atia.raji@gmail.com; noboru@nagaokaut.ac.jp).

Color versions of one or more of the figures in this paper are available online at http://ieeexplore.ieee.org.

Digital Object Identifier 10.1109/TSG.2016.2519541

D	Duty cycle, or the period of time that all schedulable appliances have to be committed once within (h).
$u(t)$	Binary variable expressing the grid power flow state (1 for purchasing and 0 for selling) at t.
$WT_{Aq}, WT_{O\&M}$	Annualized acquisition and operating costs of WT ($/kW).
$Z_{t,m}$	Binary factor expressing the occurrence possibility of Task m at t.
Z_B	Degradation factor of the considered battery technology.
A	Set of all shiftable appliance types available in the microgrid.
T	Set of hours (time horizon) in the optimization problem.
H_i, H_m	Shifting time windows of appliances type i, m.
$\eta_{AC/DC}, \eta_{DC/AC}$	Energy conversion efficiency from AC to DC and vice versa.
η_r	Battery roundtrip efficiency.

II. Introduction

CONVENTIONAL power generation systems use fossil fuels as a primary source of electricity, yet these finite natural resources are known to be the dominant producers of greenhouse gases. In order to reduce harmful emissions and meet the increased global electricity demand, renewable energy sources (RESs) are introduced as future replacements. The intensive research and development in this field has led to a huge growth in RES installations that are driven by cost decreases [1], [2]. However, the irregularity of RESs, and the limitations of available battery energy storage system (BESS) technologies prevent a high level of RES integration. Hybrid renewable energy systems (HRESs), comprising different renewable energy technologies in one design, are helpful since they provide a higher balance in energy supply as compared to a single-source system.

Smart grids (SGs), which are perceived as next generation power systems, provide two-way communication channels between energy generation sources and end users [3], and allow the shift of demand to off-peaks or to renewable generation periods. This offers reduced operations and management costs for utilities, lower power costs for consumers, and ultimately, reduced emissions [4]. Furthermore, the recent increase in the use of electric vehicles (EVs) will increase electricity demands, but at the same time will increase energy demand flexibility by the control of EVs charge periods and other vehicle-to-grid applications [5], [6]. Due to these facts, the planning, operation, and management of future power systems will not be identical to those of conventional power systems, where all of the involved technologies should be considered in the design stage.

The literature reporting the problem of sizing RESs, can be classified in two main categories. The first category includes integrating RESs into conventional power systems where the smart control of the electric load is not considered, and it has received the most attention in the available literature. Here, we include and review some of them [7]–[13]. For example, Alsayed *et al.* [7] presented a multi-criteria decision making algorithm for sizing a PV-wind system that satisfies a certain balance of economic, environmental, and social factors. Reference [10] also presented a multi-criteria sizing algorithm that was solved using a particle swarm optimization method. The sizing algorithm introduced in [13], adopted a novel power filter for limiting the fluctuation of renewable generation, and thus improve the stability of the electric grid.

The second category pays attention to integrating RESs with SGs, where the potential role of EVs and other flexible electric loads for accommodating higher levels of renewables are highlighted. Some related literature is found in [14]–[19]. Reference [14] proposed a stochastic method, based on a Monte Carlo simulation and particle swarm optimization, for sizing a smart household energy system which takes into consideration the demand uncertainty. Another stochastic based optimization that accounts for load shifting is presented in [15]. Regarding the EV utilization in power system application, the effect of different EV control strategies in reducing surplus wind generation and harmful emissions was investigated [16]. A study investigating EV effect in high PV penetration scenarios is found in [17]. However, in the majority of the aforementioned studies, which were set for long-term evaluation, the energy management of the system is rule-based, i.e., it employs a predefined operation strategy, which means that it might not be optimal.

On the other hand, the short-term scheduling of SG to achieve optimal control of energy dispatch and demand side management (DSM) in daily operation scenarios has been the main focus of [20]–[27]. In light of this, the current work introduces a reliable and efficient framework for optimizing HRES with BESS for supplying residential microgrids based on intelligent management. Fig. 1 shows a general block diagram of the proposed system. It utilizes PV and wind turbine (WT) generators as its renewable sources, a BESS, and a bi-directional inverter for converting energy from AC to DC (and vice versa). The electric demand features controllable and non-controllable loads.

The novelty of this work lies in developing an integrated model that accounts for the different aspects and characteristics of energy consumption in modern power systems. More importantly, the load flexibility gained by using smart grid demand response programs, that enable the scheduling of high energy-consuming appliances such as washing machines, cloth driers, dish washers, and EVs in aims to benefit the users rather than treating them as randomly committed appliances.

Therefore, it coincides with the principle of a smart grid operation. The model can be applied to large-scale design cases including numerous operation patterns, without imposing high computational burdens. In order to estimate all electricity consumption aspects, TRNSYS software is used to simulate the dynamic thermal behavior of residential buildings, and predict the required electric energy for supplying the thermal load, which partly contributes to the non-controllable load of the residential community. Furthermore, the uncertainty in prediction of electric load and renewable energy resources are

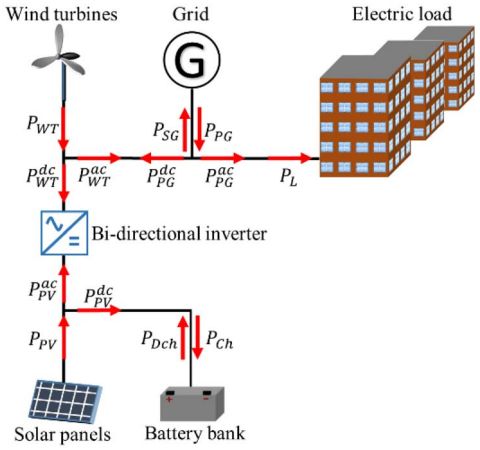

Fig. 1. Block diagram of the contemplated system.

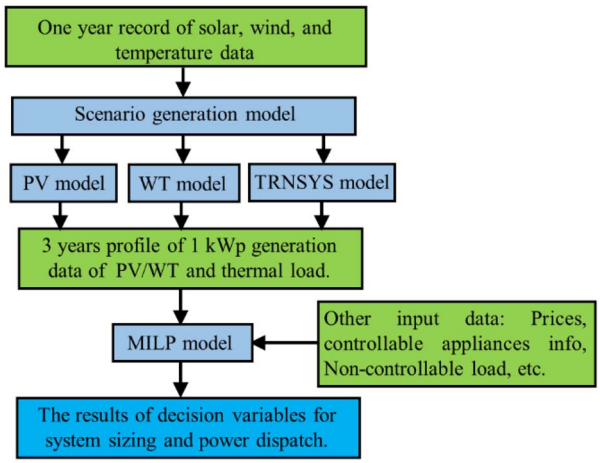

Fig. 2. Framework of the optimization process.

described by proper probability distribution functions (PDFs), and introduced into the optimization using scenario generation techniques. The optimization method employs mixed integer linear programming (MILP) since it can solve long-term scheduling problems by satisfying all restrictions and guaranteeing the optimal power management of the microgrid, where other heuristic optimization methods combined with simple power management strategies might fail. The MILP model is generated for three years and solved using the high-performance IBM ILOG CPLEX Optimization software that returns the decision variables: PV, WT, BESS, and inverter capacities, in addition to the hourly power dispatch decisions along the optimization horizon. The proposed optimization method can be used for planning new systems, or for upgrading systems already in operation to ensure that the growing electrical demand is efficiently served. A case study of a residential community in Okinawa, Japan is proposed to discuss the effect of load flexibility on component sizing, and other aspects of the system under different scenarios of operation and uncertainty.

III. Optimization Model and Formulation

Fig. 2 shows the general framework of the optimization process that starts by feeding the available one-year weather data record into stochastic models for generating three-year long weather data. The generated data is then fed into the PV, WT, and TRNSYS models to predict the hourly power generation from 1 kW PV and WT, and the thermal profile of the residential buildings. These profiles, in addition to other data, are introduced to an MILP model, to optimize the system design. The formulation of the model is displayed next, where the considered discrete time step is one hour ($\Delta t = 1$), and for ease it will be dropped from all formulas.

A. Energy Balance

The power dispatched from the WT, PV, and the grid/diesel genset, are represented by two components each, as shown in Fig. 1. The energy balance is preserved by applying two equations: one for the AC bus and another for the DC bus, at each hour $t \in T$, as in the following:

$$P_{WT}^{ac}(t) + \eta_{DC/AC}\left[P_{PV}^{ac}(t) + P_{Dch}(t)\right] + P_{PG}^{ac}(t) = P_L(t) + P_{SG}(t) \quad (1)$$

$$\eta_{AC/DC}\left[P_{WT}^{dc}(t) + P_{PG}^{dc}(t)\right] + P_{PV}^{dc}(t) = P_{Ch}(t) \quad (2)$$

Given that renewable energy resources are highly irregular and under high-penetration renewables, the renewable generation can be much higher than the power consumption, and thus the ability for curtailing renewable generation in such cases is implemented by using the following constraints that limits the dispatched power by the maximum available generation at that hour:

$$P_{WT}^{ac}(t) + P_{WT}^{dc}(t) \le N_{WT} \cdot P_{WT_1}(t) \quad (3)$$

$$P_{PV}^{ac}(t) + P_{PV}^{dc}(t) \le N_{PV} \cdot P_{PV_1}(t) \quad (4)$$

The purchased/sold power should not exceed the substation capacity or the maximum contracted power:

$$P_{PG}^{ac}(t) + P_{PG}^{dc}(t) \le u(t) \cdot \overline{P_G} \quad (5)$$

$$P_{SG}(t) \le (1 - u(t)) \cdot \overline{P_G} \quad (6)$$

Generally, the variable u is used to restrict the simultaneous purchasing and selling of power since it is perceived as a profitable solution (help minimizing the objective function) when selling prices are higher than the purchasing prices, and it is the only binary variable in the formulation. Accordingly, this variable is not needed if the simultaneous purchasing and selling is not profitable, and the problem can be formulated as linear programming rather than MILP.

P_{WT_1} is calculated as a piece-wise function of the wind speed v and the wind turbine related parameters as follows [6]:

$$P_{WT_1}(t) = \begin{cases} 0, & if\ v(t) < v_{ci}\ or\ v(t) > v_{co} \\ \dfrac{v^3(t) - v_{ci}^3}{v_r^3 - v_{ci}^3} & if\ v(t) > v_{ci}\ \&\ v(t) < v_r \\ 1, & if\ v(t) > v_r\ \&\ v(t) < v_{co} \end{cases} \quad (7)$$

where v_{ci}, v_r, and v_{co} are the cut-in, rated, and cut-out wind speeds. Given that these parameters are highly dependent on the WT size, a 50 kW WT, which is considered proper for

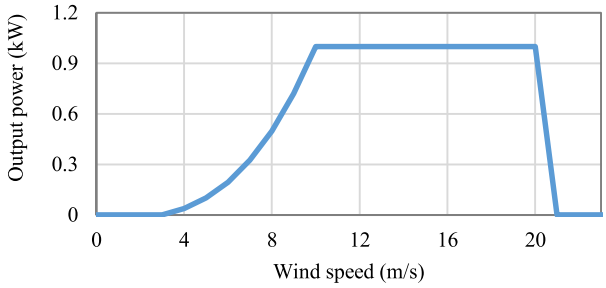

Fig. 3. Output power curve of an equivalent 1 kW WT.

the objective design, was chosen. The parameters values are 3, 10, and 20 m/s for v_{ci}, v_r, and v_{co}, respectively, and the resulted power curve is shown in Fig. 3. Generally, the search space for WT size is not continuous (integer), however, the optimized size can be roughly met using different size combinations of available commercial WTs. Therefore, and for acceptable tolerance, N_{WT} was treated as a continuous variable. P_{PV_1} is calculated as a function of the incident global solar radiation I_G and ambient temperature T_a as follows [28]:

$$T_c(t) = T_a(t) + I_G(t)\frac{NOCT - 20}{0.8} \tag{8}$$

$$P_{PV_1}(t) = Y_d \frac{I_G(t)}{I_S}\left[1 - \frac{K_p}{100}(T_c(t) - T_{STC})\right] \tag{9}$$

where T_c: cell temperature (°C), $NOCT$: nominal operating cell temperature (°C), Y_d: Derating factor due to dust accumulation, I_S: standard radiation (kWh/m^2), K_p: Power temperature coefficient (%/°C), T_{STC}: cell temperature at standard test conditions (°C). The incident global radiation depends on the solar panel tilt angle, and thus Meteonorm software was used to calculate the radiation at 30° tilted surfaces, which is considered optimal in the objective location.

B. Battery Charge and Discharge Model

This group of constraints guarantees that the battery operation model will match the power and energy charge/discharge limitations.

The energy change of the battery over one hour is given as

$$Q_B(t+1) = Q_B(t) + \eta_r P_{Ch}(t) - P_{Dch}(t) \tag{10}$$

The stored energy is restricted by the minimum and maximum allowed SOC as follows:

$$Q_B(t) \le \overline{SOC} \cdot N_B - Q_f(t) \tag{11}$$

$$Q_B(t) \ge \underline{SOC} \cdot N_B \tag{12}$$

where Equation (11) considers the battery capacity fading with use, which is often assumed proportional to the discharge energy drained from battery through time [29]. At any given hour, the total capacity fade is expressed as:

$$Q_f(t+1) = Q_f(t) + Z_B \cdot P_{Dch}(t) \tag{13}$$

where Z_B is the linear degradation factor that was analyzed for different battery technologies, based on long-term field measurement of BESS in [30].

At the end of the time horizon, the stored energy should be larger than the initial stored energy to ensure that all of the energy cost is evaluated:

$$Q_B(|T|) \ge SOC_0 \cdot N_B \tag{14}$$

Charge and discharge power are limited in each time step as following:

$$P_{Ch}(t) \le N_B \cdot \overline{P_B} \tag{15}$$

$$P_{Dch}(t) \le N_B \cdot \overline{P_B}. \tag{16}$$

C. Inverter Model

The nominal capacity of the bi-directional inverter is formulated to be greater than any electric power that can pass through in both directions:

$$\eta_{DC/AC}\left[P_{Dch}(t) + P_{PV}^{ac}(t)\right] \le N_{Inv} \tag{17}$$

$$\eta_{AC/DC}\left[P_{WT}^{dc}(t) + P_{PG}^{dc}(t)\right] \le N_{Inv}. \tag{18}$$

D. Load Model

Three main parts of the load are considered:

i. Thermal load: The main reason for energy consumption change from season to season. Thus, TRNSYS software is used to predict the yearly thermal load required for a typical 100 m^2 one-story Japanese house in Okinawa. A range of 22–27 Celsius is maintained daily between 07:00 and 23:00 for a 50 m^2 effective heating/cooling area. The outer walls feature heat-insulating layers, and the house is naturally ventilated at an hourly rate of 0.6. The one house generated profile, shown in Fig. 4, is scaled due to the number of houses in order to express the total thermal load in the microgrid. In Okinawa, the required thermal load mainly results from cooling the buildings in hot weather. Accordingly, the thermal load is fully supplied by electric heat pumps, where the corresponding electric consumption can be calculated after estimating the hourly coefficient of performance (COP) of the residential heat pump, defined as the ratio of heating or cooling provided to electrical energy consumed, based on the ambient and indoor temperature that resulted from the simulation and shown in Fig. 5.

ii. Non-controllable appliances: Every house has uncontrollable electric appliances devoted to users' habits and their needs, such as cooking appliances, hair dryers, vacuum cleaners, lighting, computer, etc. These Non-controllable appliance consumption, in addition to the thermal load, form the total non-controllable load, P_{NCL}.

iii. Controllable load: Table I, lists some high consumption appliances in the residential sector. These appliances can be committed within different shifting time windows that are chosen to accommodate residential consumers, even without using automated self-scheduling devices. Domestic water heaters can also be considered as a controllable appliance. However, in Okinawa, a solar assisted heating system, coupled with gas-powered heaters are more efficient and widely used. Thus, it is not included in our case. Table I also lists

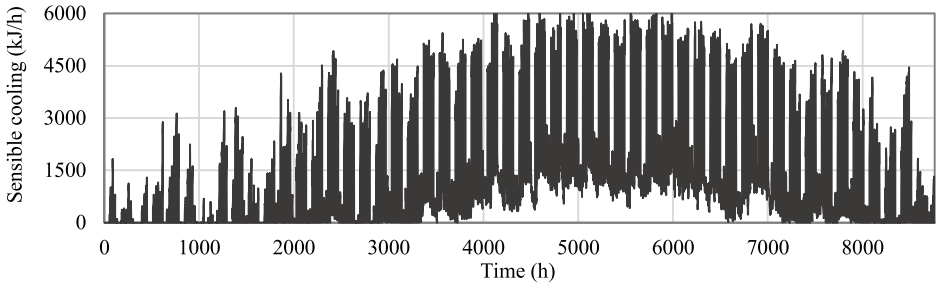

Fig. 4. Yearly sensible cooling profile for a 100 m^2 family house in Okinawa.

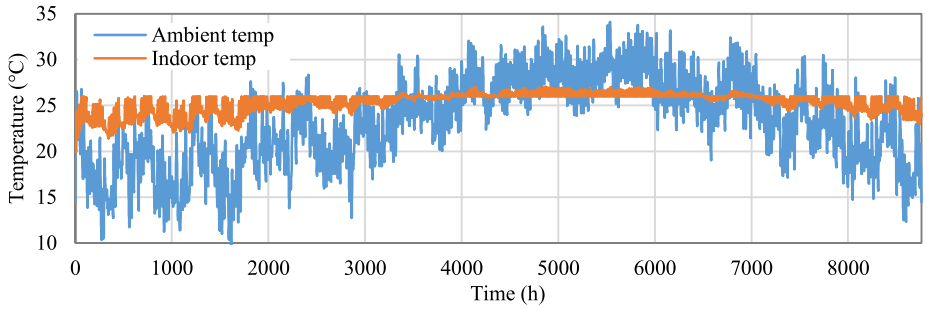

Fig. 5. Yearly ambient and indoor temperature simulation.

three different patterns of EVs charging time windows. The first and second patterns, denoted as EV1 and EV2, represents those people who are committed to their daily jobs, and are disconnected from the grid between 7:00–18:00. EV1 can utilize the cheap charging rates during the early morning hours, whereas EV2 represents people with more strict needs that they charge during the evening time. EV3 features homemakers and non-employed people patterns, where their vehicles stay connected to the microgrid during most of the day. The usage frequency indicates how often a certain appliance type is used every day, but in the case of EV, the usage frequency represents the percent of each pattern.

The developed load model ensures the representation of all of the aforementioned load parts by aggregating the whole operation patterns, without requiring modeling each type of appliance as a new variable in the optimization. This reduces the problem size and the required optimization time. The model is expressed by the following constraints:

For each appliance type $i \in A$, the total electric load during its shifting time window H_i, should be larger than the minimum electric consumption, due to the mandatory occurrence of some tasks in addition to the non-controllable load within H_i. This relation is applied every D hour along T:

$$\sum_{t \in H_i} P_L(t) \geq \sum_{m \in A} N_{App}^{m} P_{App}^{m} D_{App}^{m} F_{i,m} + \sum_{t \in H_i} P_{NCL}(t) \quad (19)$$

In the above equation, $F_{i,m}$ represents the ratio of the minimum operation time of appliance type m during H_i to the task duration D_{App}^{m}, and it can be calculated as:

$$F_{i,m} = 1 - min\left\{\frac{K_{i,m}}{D_{App}^{m}}, 1\right\} \quad (20)$$

TABLE I
CONSIDERED APPLIANCES AND THEIR SPECIFICATIONS

Appliance	Power (kW)	Duration (h)	Usage Freq	Shifting window
Washing machine	0.5	1	0.7	[07:00–24:00]
Cloth dryer	1	1	0.7	[07:00–24:00]
Dish washer	0.9	1	1	[18:00–24:00]
EV1	2	3	0.4	[00:00–07:00]
EV2	2	3	0.3	[18:00–24:00]
EV3	2	3	0.3	[00:00–24:00]

where $K_{i,m}$ represents the maximum number of consecutive hours of $H_m \backslash H_i$ for an appliance of type m, that has to be operated continuously (such as the operation of washing machines), or it can also represent the number of total hours of $H_m \backslash H_i$ for an appliance m that can be operated discretely (such as the charging of an EV). It should be noted that if there were two different types of appliances that share the same shifting window, they would have the same constraints. In other words, this set is required only once for each different shifting window, which reduces the problem size.

The second constraint limits the minimum consumption at each $t \in T$ to the non-controllable load required at each step:

$$P_L(t) \geq P_{NCL}(t) \quad (21)$$

The following constraint guarantees that the total consumption every D hour along T equals the expected total load:

$$\sum_{t=1}^{D} P_L(t) = \sum_{m \in A} N_{App}^{m} P_{App}^{m} D_{App}^{m} + \sum_{t=1}^{D} P_{NCL}(t) \quad (22)$$

Given that some appliance types require several hours to commit to their tasks, such as EV that requires 3×2 kWh as shown in Table I, and in order to prevent solutions that

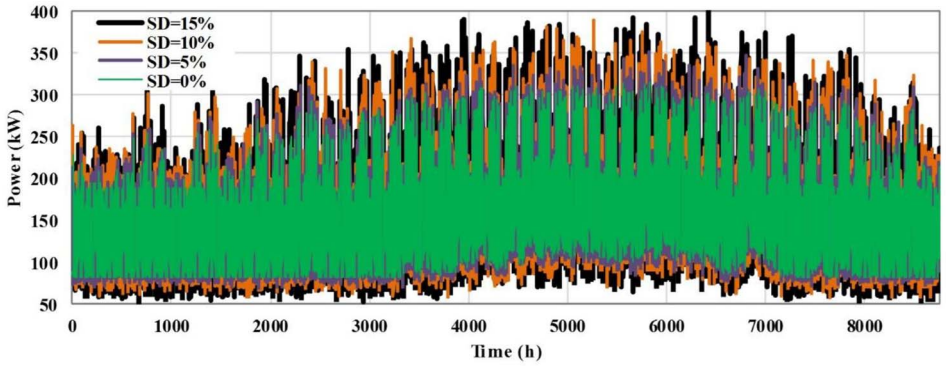

Fig. 6. Yearly expected load along with other scenario generated profiles corresponding to different uncertainties.

accumulate the required energy for the appliance into one time slot, i.e., 1×6 kWh in case of EV, the following constraint is added:

$$P_L(t) \leq \sum_{m \in A} N_{App}^{m} P_{App}^{m} Z_{t,m} + P_{NCL}(t) \tag{23}$$

where $Z_{t,m}$ is defined as

$$Z_{t,m} = \begin{cases} 1 & if\ t \in H_m \\ 0 & if\ t \notin H_m. \end{cases} \tag{24}$$

E. Economic Model

The objective function minimizes the annualized cost of the system (ACS), which includes the acquisition, operation and maintenance (O&M), replacement, and power purchasing costs of the grid, while maximizing the profit of selling power to the grid. The cost function is written as:

$$\begin{aligned} ACS = {} & N_{PV}\left(PV_{Aq} + PV_{O\&M}\right) + N_{WT}\left(WT_{Aq} + WT_{O\&M}\right) \\ & + N_{Inv}\left(Inv_{Aq} + Inv_{O\&M} + Inv_{Rep}\right) \\ & + N_B\left(B_{Aq} + B_{O\&M}\right) + Q_f(|T|)B_{Rep} \\ & + \sum_{t \in T}\left[C_P(t)\left(P_{PG}^{ac}(t) + P_{PG}^{dc}(t)\right) - C_S(t)P_{SG}(t)\right] \end{aligned} \tag{25}$$

where in the above formula, the term $Q_f(|T|)B_{Rep}$ represents the battery value loss due to capacity fade, and it is expressed as the product of battery capacity loss at the end of the optimization horizon and the replacement cost. PV and WT have no replacement costs, whereas one replacement is necessary for the inverter during the project lifetime. The price of power purchasing and selling should be considered according to the local power legislation and the tariff of the design location.

F. Stochastic Model

Renewable energy resources like solar radiation and wind have an intrinsic stochastic behavior that leads to remarkable variation from one year to another. This may badly affect the optimization quality. Therefore, the scenario generation method, a well-known strategy for modeling stochastic behavior, is used to generate several years of weather data, and is solved as a deterministic model. Weather data is highly dependent on the daytime and season, therefore, the yearly data records are classified into 12 sets, one for each month, and then every set is sorted into 24 subsets, where each subset corresponds to one hour of the day. The subsets are fit into proper probability distribution functions (PDFs), Gaussian for solar radiation, and Weibull for wind speed [14], in order to obtain 24 fits for solar radiation and other 24 fits for wind speed for each month of the year. In addition, there is a high uncertainty involving the prediction of electric load due to the variation of habits, or due to the lack of information. For example, families tend to heat/cool different space sizes of their homes, leading to a deviation of the 50 m^2 value that we considered in the TRNSYS simulation as the effective cooling area. Furthermore, large microgrids combine various house and building designs that are difficult to account individually, and in order to deal with such uncertainties, the expected non-controllable load is subjected to a Gaussian PDF, where its median value is the hourly expected load, and its standard deviation (SD) is considered in a way that reflects the involved uncertainty. Fig. 6 shows the yearly expected load profile of the microgrid (SD = 0%), along with other scenario generated profiles corresponding to different uncertainties. In the proposed case study, the uncertainties effect on the system design is analyzed.

IV. Case Study

A residential microgrid in Okinawa that features an average daily demand of 4000 kWh was considered, where an average household daily consumption in this area is around 15 kWh [31]. We expressed the load flexibility by the percent of controllable demand to total demand, denoted as Per_{CL}. Regarding Table I, a Per_{CL}= 15% can be roughly achieved by scheduling the first three types of electric appliances. With consideration of one EV per house, this might reach up to more than 40%. This is an average estimation, where in summer, Per_{CL} decreases due to higher thermal load, whereas in winter it increases. In order to show the load flexibility effect on the optimal design, several values of Per_{CL} were considered: 0, 15, 30, and 45%. Per_{CL}= 0% represents the conventional design case, where there is an absence of demand response programs. Per_{CL}=15% considers mainly the demand management of house appliances with some EVs if required to achieve the percentage. Per_{CL}= 30 and 45% emulate 60 and 100% of

TABLE II
ECONOMIC DATA OF THE SYSTEM COMPONENTS

Initial acquisition costs				Initial replacement costs		Yearly O&M costs
PV ($/kW)	WT ($/kW)	Battery ($/kWh)	Inverter ($/kW)	Battery ($/kWh)	Inverter ($/kW)	2% of initial acquisition costs
3000[1]	2500[2]	195	500	195	500	

TABLE III
TECHNICAL DATA AND CONSTANTS VALUES

Nominal interest rate (%)	Inflation rate (%)	Project lifetime (years)	$\overline{P_B}$ (kW)	$\underline{SOC}$	$\overline{SOC}$	SOC_0	Z_B (lead-acid type)	$\eta_{DC/AC}$	$\eta_{AC/DC}$	η_r
3.75	1.5	25	0.5	0.2	0.95	0.5	3.10^{-4}[29]	0.93	0.93	0.86

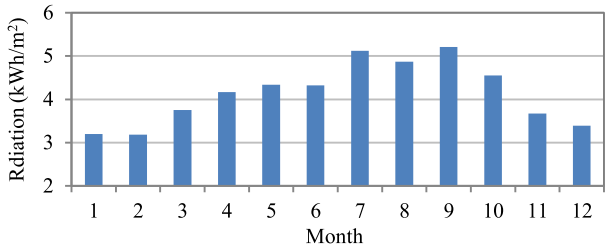

Fig. 7. Monthly average daily global radiation at 30° tilted surface.

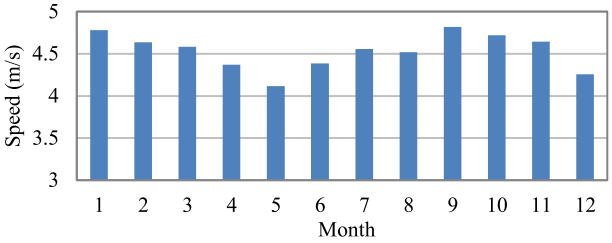

Fig. 8. Monthly average wind speed.

EV adoption per family, respectively. Since we want to analyze the system sizing of these cases under equal total demand, and since owning an EV will increase the consumption per household, the number of consumers in each case is manipulated in accordance to the EVs number. For example, for Per_{CL}= 0 and 15%, the number of consumers is 266, while for Per_{CL}= 30 and 45%, the number of consumers are 215 and 190, respectively.

Tables II and III report economic and technical data, and the other parameters that were considered during optimization of the case study. The considered electricity time of use rates is 0.32 $/kWh from 7:00 to 23:00, and 0.12 $/kWh for any other time in accordance to Tokyo Electric Power Company [32]. Fig. 7-8 shows the monthly average global daily radiation and wind speed at the objective location, respectively.

The load flexibility effect was analyzed according to five scenarios, where each optimization was carried for three years long model. These scenarios and their optimization results are reported below:

Scenario 1: In this scenario, it is considered that the system can utilize all resources PV, WT and BESS, and the surplus energy generated can be sold to the grid at a 20% reduced price of the purchase rates to account for transmission loss. Table IV shows the corresponding optimization results. Battery size shows a high trend against Per_{CL}, where it decreases, with increases in the Per_{CL} due to the augmented ability to align the consumption to renewable generation or off-peak periods. In cases of less flexibility, it is more economical to store the renewable generation, then restore it when demanded, which requires an increased BESS size. The increased flexibility of the load can help better accommodating the fluctuant wind generation, and therefore, the optimized WT size increases whereas the PV size decreases when there is more flexibility to shift the load toward the WT generation time. However, this feature is limited due to the irregularity of renewable generation over the year. Fig. 9 shows a one-day simulation for the energy dispatch every hour, where it can be seen that the power is purchased during the late night and early morning cheap rates and used to charge the battery and supply the load, and during the high electricity rates, the battery is discharged to supply the load and grid (selling). During the noontime when there is high renewable generation, the shiftable load and the battery are used to absorb the surplus generation that cannot be fed to the grid due to the limited substation capacity. Some parts of the load are also shifted to cheap rate periods within the control limits. It is clearly seen that the MG optimal operation is complicated and requires comprehensive planning for a several-day period, which cannot be accurately depicted by simple power dispatch strategies.

TABLE IV
OPTIMIZATION RESULTS OF SCENARIO 1

Per_{CL} (%)	0	15	30	45
N_{WT} (kW)	432	475	525	550
N_{PV} (kW)	1213	1142	1083	986
N_B (kWh)	2169	1826	1740	1592
N_{Inv} (kW)	423	390	357	318
Cost ($)	243000	237000	230000	224000

Scenario 2: Considering the limitation to deploy large capacities of RESs in many real-world design cases, this scenario focuses on sizing the system for matching the need of the microgrid, while neglecting the profits of surplus generated power that can be sold to the grid. Table V shows the corresponding results where the optimal capacities of all components are much less than the corresponding ones

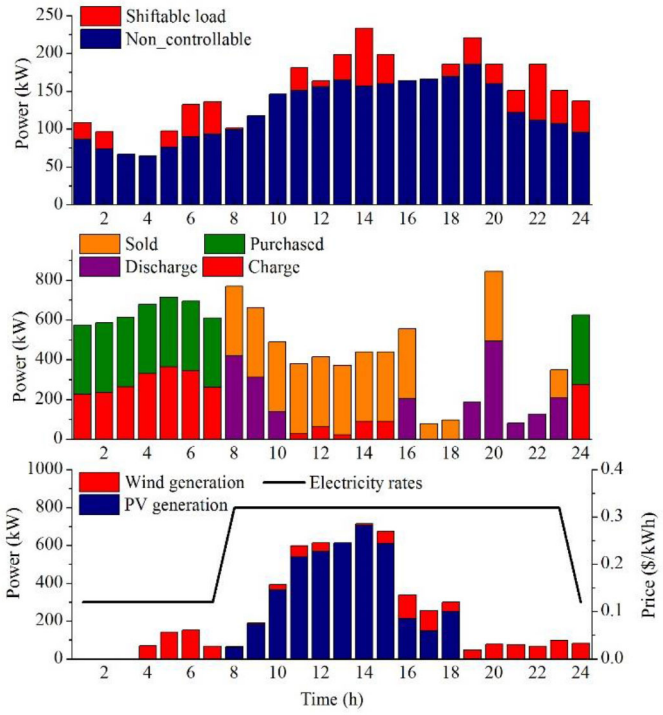

Fig. 9. One day simulation of scenario 1.

TABLE V
OPTIMIZATION RESULTS OF SCENARIO 2

Per_{CL} (%)	0	15	30	45
N_{WT} (kW)	132	135	175	185
N_{PV} (kW)	532	524	486	450
N_B (kWh)	1500	1070	1014	936
N_{Inv} (kW)	232	196	151	129
Cost ($)	295000	286000	277000	269000

TABLE VI
OPTIMIZATION RESULTS OF SCENARIO 3

Per_{CL} (%)	0	15	30	45
N_{WT} (kW)	245	222	275	270
N_{PV} (kW)	382	365	287	233
N_B (kWh)	100	100	100	100
N_{Inv} (kW)	185	176	138	109
Cost ($)	347000	322000	304000	289000

in scenario 1. The same trend of capacity change against load flexibility as in scenario 1 is also observed.

Scenario 3: In addition to limiting the surplus energy selling, this scenario explores the load flexibility effect under limited BESS. Therefore, only a 100 kW of BESS is assumed to attenuate the power fluctuation of RESs. As shown in Table VI, and compared to scenario 2, the optimized systems utilize higher capacities of WT and lower capacities of PV that is interpreted by a higher trend to use augmented integral characteristics of WT and PV generation when an energy storage system is not available. Comparing the annualized cost change of the system against Per_{CL} to those in the previous scenarios, it can be observed that it is much higher in scenario 3, indicating the potential achievable savings when using demand response programs without BESS.

TABLE VII
OPTIMIZATION RESULTS OF SCENARIO 4 FOR SD = 10%

Per_{CL} (%)	0	15	30	45
N_{WT} (kW)	377	450	525	545
N_{PV} (kW)	1230	1136	1071	1019
N_B (kWh)	2165	1888	1712	1636
N_{Inv} (kW)	427	391	355	326
Cost ($)	243000	232000	229000	226000

TABLE VIII
OPTIMIZATION RESULTS OF SCENARIO 4 FOR SD = 15%

Per_{CL} (%)	0	15	30	45
N_{WT} (kW)	403	455	526	502
N_{PV} (kW)	1192	1128	1038	1062
N_B (kWh)	2262	1901	1689	1720
N_{Inv} (kW)	428	390	348	333
Cost ($)	238000	228000	228000	226000

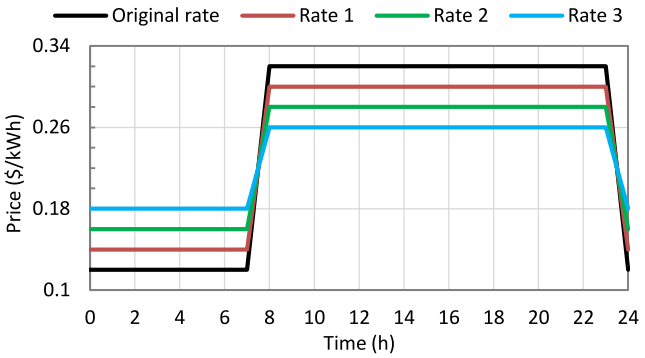

Fig. 10. Assumed electricity rates with more flattened patterns.

Scenario 4: In the first three scenarios, a 5% of standard deviation was considered for incorporating the effect of electric load uncertainty. In this scenario, higher uncertainties are contemplated to analyze the system sizing of new residential areas, where a good prediction is not available. Therefore, scenario 1 is optimized again under 10% and 15% standard deviations, and the corresponding results are shown in Table VII and Table VIII, respectively. Even with higher uncertainties, the component sizing results are generally in good agreement with those corresponding to 5% (Table IV), indicating that the proposed sizing method has a good and reliable performance. However, the achievable cost saving against Per_{CL} increase is generally irregular and negligible in some points as it is displayed in Table VIII between Per_{CL}=15% and Per_{CL}=30%. Repeating the optimization for several times can result in a more uniform cost prediction in such cases involving large uncertainties.

Scenario 5: The impact of the utility pricing policy on the system design is analyzed in this scenario. Since the original electricity rate analyzed in previous scenarios has an attractive on/off peak price margin (0.2 $/kWh), three rates with smaller margins are assumed as shown in Fig. 10 along with the original rate. All these rates are symmetrical around the value 0.22 $/kWh and the lowest on/off peak margin is 0.08 $/kWh. Scenario 1 with Per_{CL}=15% is again optimized according to these rates, and the results are displayed in table IX. With a smaller on/off peak margin, the battery size

TABLE IX
OPTIMIZATION RESULTS OF SCENARIO 5

	Original rate	Rate 1	Rate 2	Rate 3
N_{WT} (kW)	475	565	675	700
N_{PV} (kW)	1142	960	650	475
N_B (kWh)	1826	1450	1005	690
N_{inv} (kW)	390	345	230	165
Cost ($)	237000	263000	290000	302000

decreases significantly as expected due to lower peak-shaving profits. However, the most remarkable point is that the PV size decreases, whereas WT size increases with lower on/off margins. This is attributed to the fact that PV generation always coincides with the on-peak price, while the wind generation is distributed throughout all durations. Therefore, when the rates gradually become more flattened, PV generation loses its advantage while wind generation becomes more effective. Furthermore, the power supply costs are expected to increase noticeably with such rates.

Matlab software was used for generating the stochastic models and the MILP matrices. Then, the models were solved by CPLEX optimization engine as a deterministic problem consuming about 90 min per instance.

V. CONCLUSION

Regarding the accelerated development of eco-friendly technologies such as RES, SG, and EV, which are finding increased economic and social acceptance, planning an efficient electric power system requires consideration of these technologies in the design stage. Therefore, we introduced a method for sizing an HRES operating within the frame of a smart grid that coherently considers the electric demand flexibility offered by DSM. Contemplating a case study for a residential microgrid in Okinawa, we studied the effect of demand flexibility on HRES sizing and estimated the potential economic benefit of such applications under different scenarios. Generally, the optimal components sizing was affected by demand flexibility and strongly affected by operational conditions (scenarios), asserting the potential use of the introduced method in modern smart grid design. The observed benefits gained by demand flexibility were encouraging for the increased adoption of SG technology, especially when there are limitations to using BESS.

In this study, our focus was limited to EV as consuming elements, where their potential use in vehicle-to-grid application was not considered. In future research, we will integrate vehicle-to-grid application after developing a proper model for accounting to the performance of embedded lithium-ion battery, as this can result in a more economically and environmentally efficient system.

REFERENCES

[1] D. Feldman *et al.*, "Photovoltaic (PV) pricing trends: Historical, recent, and near-term projections," U.S. Dept. Energy, Washington, DC, USA, Tech. Rep. DOE/GO-102012-3839, Nov. 2012.

[2] R. Wiser, E. Lantz, and M. Hand, "WREF 2012: The past and future cost of wind energy," U.S. Dept. Energy, Washington, DC, USA, Tech. Rep. LBNL-5421E, Mar. 2012.

[3] V. C. Güngör *et al.*, "Smart grid technologies: Communication technologies and standards," *IEEE Trans. Ind. Informat.*, vol. 7, no. 4, pp. 529–539, Nov. 2011.

[4] C.-H. Lo and N. Ansari, "The progressive smart grid system from both power and communications aspects," *IEEE Commun. Surveys Tuts.*, vol. 14, no. 3, pp. 799–821, Jul. 2011.

[5] W. Kempton and J. Tomić, "Vehicle-to-grid power implementation: From stabilizing the grid to supporting large-scale renewable energy," *J. Power Sources*, vol. 144, no. 1, pp. 280–294, Jun. 2005.

[6] T. Wu, Q. Yang, Z. Bao, and W. Yan, "Coordinated energy dispatching in microgrid with wind power generation and plug-in electric vehicles," *IEEE Trans. Smart Grid*, vol. 4, no. 3, pp. 1453–1463, Sep. 2013.

[7] M. Alsayed, M. Cacciato, G. Scarcella, and G. Scelba, "Multicriteria optimal sizing of photovoltaic-wind turbine grid connected systems," *IEEE Trans. Energy Convers.*, vol. 28, no. 2, pp. 370–379, Jun. 2013.

[8] R. Atia and N. Yamada, "Optimization of a PV-wind-diesel system using a hybrid genetic algorithm," in *Proc. IEEE Elect. Power Energy Conf.*, London, ON, Canada, 2012, pp. 80–85.

[9] R. Chedid and S. Rahman, "Unit sizing and control of hybrid wind-solar power systems," *IEEE Trans. Energy Convers.*, vol. 12, no. 1, pp. 79–85, Mar. 1997.

[10] M. Sharafi and T. Y. ELMekkawy, "Multi-objective optimal design of hybrid renewable energy systems using PSO-simulation based approach," *Renew. Energy*, vol. 68, pp. 67–79, Aug. 2014.

[11] R. Huva, R. Dargaville, and S. Caine, "Prototype large-scale renewable energy system optimisation for Victoria, Australia," *Energy*, vol. 41, no. 1, pp. 326–334, May 2012.

[12] Y. A. Katsigiannis, P. S. Georgilakis, and E. S. Karapidakis, "Hybrid simulated annealing—Tabu search method for optimal sizing of autonomous power systems with renewables," *IEEE Trans. Sustain. Energy*, vol. 3, no. 3, pp. 330–338, Jul. 2012.

[13] L. Xu, X. Ruan, C. Mao, B. Zhang, and Y. Luo, "An improved optimal sizing method for wind-solar-battery hybrid power system," *IEEE Trans. Sustain. Energy*, vol. 4, no. 3, pp. 774–785, Jul. 2013.

[14] S. Kahrobaee, S. Asgarpoor, and W. Qiao, "Optimum sizing of distributed generation and storage capacity in smart households," *IEEE Trans. Smart Grid*, vol. 4, no. 4, pp. 1791–1801, Dec. 2013.

[15] A. Arabali, M. Ghofrani, M. Etezadi-Amoli, and M. S. Fadali, "Stochastic performance assessment and sizing for a hybrid power system of solar/wind/energy storage," *IEEE Trans. Sustain. Energy*, vol. 5, no. 2, pp. 363–371, Apr. 2014.

[16] L. Göransson, S. Karlsson, and F. Johnsson, "Integration of plug-in hybrid electric vehicles in a regional wind-thermal power system," *Energy Policy*, vol. 38, no. 10, pp. 5482–5492, Oct. 2010.

[17] Q. Zhang, T. Tezuka, K. N. Ishihara, and B. C. Mclellan, "Integration of PV power into future low-carbon smart electricity systems with EV and HP in Kansai area, Japan," *Renew. Energy*, vol. 44, pp. 99–108, Aug. 2012.

[18] N. Juul and P. Meibom, "Optimal configuration of an integrated power and transport system," *Energy*, vol. 36, no. 5, pp. 3523–3530, May 2011.

[19] C. K. Ekman, "On the synergy between large electric vehicle fleet and high wind penetration—An analysis of the Danish case," *Renew. Energy*, vol. 36, no. 2, pp. 546–553, Feb. 2011.

[20] A. Botterud *et al.*, "Demand dispatch and probabilistic wind power forecasting in unit commitment and economic dispatch: A case study of Illinois," in *Proc. IEEE Power Energy Soc. Gen. Meeting*, Vancouver, BC, Canada, 2013, p. 1.

[21] Y. Guo, M. Pan, Y. Fang, and P. P. Khargonekar, "Decentralized coordination of energy utilization for residential households in the smart grid," *IEEE Trans. Smart Grid*, vol. 4, no. 3, pp. 1341–1350, Sep. 2013.

[22] N. Kunwar, K. Yash, and R. Kumar, "Area-load based pricing in DSM through ANN and heuristic scheduling," *IEEE Trans. Smart Grid*, vol. 4, no. 3, pp. 1275–1281, Sep. 2013.

[23] E. Matallanas *et al.*, "Neural network controller for active demand-side management with PV energy in the residential sector," *Appl. Energy*, vol. 91, no. 1, pp. 90–97, Mar. 2012.

[24] A.-H. Mohsenian-Rad and A. Leon-Garcia, "Optimal residential load control with price prediction in real-time electricity pricing environments," *IEEE Trans. Smart Grid*, vol. 1, no. 2, pp. 120–133, Sep. 2010.

[25] A.-H. Mohsenian-Rad, V. W. S. Wong, J. Jatskevich, R. Schober, and A. Leon-Garcia, "Autonomous demand-side management based on game-theoretic energy consumption scheduling for the future smart grid," *IEEE Trans. Smart Grid*, vol. 1, no. 3, pp. 320–331, Dec. 2010.

[26] A. Molderink, V. Bakker, M. G. C. Bosman, J. L. Hurink, and G. J. M. Smit, "Management and control of domestic smart grid technology," *IEEE Trans. Smart Grid*, vol. 1, no. 2, pp. 109–119, Sep. 2010.
[27] M. Vasirani, R. Kota, R. L. G. Cavalcante, S. Ossowski, and N. R. Jennings, "An agent-based approach to virtual power plants of wind power generators and electric vehicles," *IEEE Trans. Smart Grid*, vol. 4, no. 3, pp. 1314–1322, Sep. 2013.
[28] M. R. Patel, *Wind and Solar Power Systems: Design, Analysis, and Operation*, 2nd ed. New York, NY, USA: Taylor & Francis, 2006.
[29] Y. Riffonneau, S. Bacha, F. Barruel, and S. Ploix, "Optimal power flow management for grid connected PV systems with batteries," *IEEE Trans. Sustain. Energy*, vol. 2, no. 3, pp. 309–320, Jul. 2011.
[30] P. Malbranche, A. Delaille, F. Mattera, and E. Lemaire, "Assessment of storage ageing in different types of PV systems: Technical and economical aspects," in *Proc. 23rd Eur. Photovolt. Solar Energy Conf. Exhibit.*, Valencia, Spain, Sep. 2008, pp. 2765–2769.
[31] *Electrical Business Handbook*, Jpn. Agency Nat. Resour. Energy, Tokyo, Japan, 2012.
[32] Tokyo Electric Power Company. (Jun. 15 2014). *8-Hour Night Service Plan*. [Online]. Available: http://www.tepco.co.jp/en/customer/guide/ratecalc-e.html

Raji Atia received the B.S. degree from Al-Baath University, Homs, Syria, in 2009, and the M.S. degree from the Nagaoka University of Technology, Nagaoka, Japan, in 2013, where he is currently pursuing the Ph.D. degree. His research interests include modern power system modelling and optimization, and smart grid operation and management.

Noboru Yamada (M'12) received the M.S. and Ph.D. degrees in mechanical engineering from Tohoku University, Sendai, Japan, in 1996 and 1999, respectively. He is currently an Associate Professor with the Department of Mechanical Engineering, Nagaoka University of Technology. His main research interests include renewable energy systems such as photovoltaics, energy storage, and waste heat recovery.